Photoabsorption cross section of O, S, Se, and Te

C.-T. Chen and F. Robicheaux
Department of Physics, Auburn University, Auburn, Alabama 36849-5311
(Received 13 July 1994)

Photoabsorption cross sections of the ground state of four oxygen-group atoms are calculated using the eigenchannel R-matrix method. The calculation is performed in the energy range from the first to the third ionization threshold of the residual ions. The present calculations are in good agreement with experimental results except for Te. We investigate the origin for some of the generic features of the cross section. A systematic study of the convergence as a function of type of basis demonstrates the importance of the polarizability of the valence shell. The lessons learned from these atoms should be generally applicable to other columns of the periodic table.

PACS number(s): 32.80.Fb, 32.80.Dz, 31.20.Di

I. INTRODUCTION

The photoabsorption spectra of open p-shell atoms within $\sim$ 5 eV of the first threshold are rich in resonance structure due to the interacting Rydberg states attached to the different $L_cS_cJ_c$ thresholds. The resonances can have extremely small ($\sim 10^{-8}$ a.u.) widths or large widths ($\sim$ 0.02 a.u.) depending on the LSJ classification of the resonance. Accurate theoretical description of these states is difficult because of the interactions between two or more open shells and the presence of perturbing states in the midst of Rydberg series. In this paper, we focus on the description of some of the chalcogens: O, S, Se, and Te. Our motivation for this study is threefold: (1) we obtain theoretical cross sections for Se and Te and more accurate cross sections for O and S and use these theoretical spectra to classify experimental resonances. (2) We demonstrate that some aspects of complex spectra originate from simple considerations. (3) We explore the types of basis functions that are needed for accurate wave functions and thus what physical effects are important for the description of the dynamics.

Oxygen is the most studied of the chalcogen atoms. The global features of the atomic oxygen spectrum have been studied for a long time [1–5]. Classification of autoionization resonances below the $^2P^o$ threshold has been made by Huffman *et al.* [6] and Dehmer *et al.* [7]. On the theoretical side, Taylor and Burke [8], Pradhan and Saraph [9], Pradhan [10], Vesnicheva *et al.* [11], Saxon *et al.* [12], and Bell *et al.* [13] have covered a wide energy range with various approaches. A compilation and review is made by Seaton [14]. The spectrum of O differs from the other chalcogens since it consists of sharp resonances only. Because the correlation is smallest in O, the heavier chalcogens are of more interest to us.

The spectrum of S is, perhaps, the most interesting because correlation is equally strong in S, Se, and Te while complications due to relativistic effects is smallest in S. Recently, Tayal [15] has calculated the photoionization cross section of atomic sulfur using the Belfast R-matrix programs. He compared the results in detail with experiments [16–18] and other theoretical works [19,20]. Altun [21] extended the theoretical description of the spectrum based on many-body perturbation theory by including the $3s \rightarrow np$ resonances above $3s3p^4\,{}^2P^e$ threshold. While the experiments [17,18] agreed quite well, the theoretical calculations did not have very good agreement among themselves and with experiment. The disagreement of the quantum defect was as large as 0.2. Besides, all the calculations have assumed LS coupling and did not contain the $(^2D^o)nd\,{}^3P^o$ resonances below the $^2D^o$ threshold. This series, however, was observed by experiment to have intense peaks. The discrepancies between theoretical calculations and experiments and also among calculations themselves have shown the necessity for further investigation of this system. A final open question on S is the assignment of two of the Rydberg series. Tondello's [16] assignment of the $(^2D^o)ns\,{}^3D^o$ and $(^2D^o)nd\,{}^3S^o$ series was reversed by Gibson *et al.* [17] based on their considerations of the quantum defects of the two series. Joshi *et al.* [18] reexamined this designation and confirmed this interchange. They also reported a few new lines. However, Tayal [15] suggested these two series should not be reversed and agreed with the assignment of Tondello. Mendoza and Zeippen [20] and Altun [21] did not give a conclusion about this disagreement. Our calculations strongly suggest that the assignment by Tondello was the correct one.

With an open valence p shell, atomic sulfur and also other oxygen-group elements are expected to have strong correlation effects. The experiments from Refs. [17,18] have provided detailed resonance structures of atomic sulfur; we mainly compare our results to those of Gibson *et al.* [17] because their spectrum was dominated by absorption from the $^3P_2^e$ ground state and is easier for comparison because satellite absorption does not introduce complications. Similar experiments on Se and Te [22,23] are also available. We do not know of any theoretical calculations on Se and Te. The theoretical description of these atoms is extremely difficult. Correlations induced by the electrostatic interactions and the spin-orbit interaction can both affect the Rydberg states. Few theoretical methods can accurately incorporate both of these effects. Our description of Se is markedly better

than that for Te.

In Sec. III we describe briefly the eigenchannel R-matrix approach and important parameters used in this calculation. We present the total cross section and compare the autoionization levels with experiment and other calculations in Sec. IV where detailed discussions are also provided.

II. CHANNELS

Considering the photoionization from the valence p subshell of the ground state ^3P, the target states for the chalcogens in the LS-coupling scheme are $ns^2np^3\ ^4S^o$, $^2D^o$, and $^2P^o$ in order of increasing energy ($n = 2$ for O, $n = 3$ for S, $n = 4$ for Se, and $n = 5$ for Te). There are nine channels and three LS symmetries that can be excited by one photon from the ground state. They are $(^4S^o)ns$, $(^2D^o)nd\ ^3S^o$; $(^2D^o)nd$, $(^2P^o)ns, nd\ ^3P^o$; and $(^4S^o)nd$, $(^2D^o)ns, nd$, $(^2P^o)nd\ ^3D^o$. When the spin-orbit potential is ignored, the $^3S^o$ channels do not interact with the $^3P^o$ channels, which do not interact with the $^3D^o$ channels.

The breakdown of LS coupling is very striking in Se and Te. The spin-orbit interaction also plays a very important role in O and S as well because this interaction allows the decay of $^3P^o$ states below the $^2D^o$ thresholds and above the $^4S^o$ threshold. In LS coupling, the $(^2D^o)nd\ ^3P^o$ are not coupled to any continuum. The spin-orbit interaction can couple the channels mentioned above to each other and to a large number of other channels: $(^2D^o)nd$ and $(^2P^o)ns, nd\ ^1P^o$; $(^2D^o)ns, nd$ and $(^2P^o)nd\ ^1D^o$; $(^2D^o)nd$ and $(^2P^o)nd\ ^1F^o$; $(^2D^o)nd$ and $(^2P^o)nd\ ^3F^o$; $(^2D^o)nd\ ^3G^o$; $(^4S^o)ns\ ^5S^o$; and $(^4S^o)nd\ ^5D^o$. jj coupling is the proper description of the resonances when the spin-orbit interaction is large. We do not list the channels in jj coupling.

III. CALCULATIONAL METHOD

We use basically the same computer codes for this calculation as was used in previous works on different atoms [24,25]. In the previous calculations, a parametrized model potential was used to get good agreement between calculated energy levels of the target ion. Using this method for the chalcogens, the parameters of the potential are chosen to describe the closed shell of the inner core. This method could be somewhat uncertain; errors could be introduced into the calculation through the parameters of the model potential (especially if the number of experimental levels is not large).

In this work we use a different approach to describe the target state. We first perform a Hartree-Fock (HF) [26] calculation to obtain one-electron orbitals of the configuration average 1+ target ion. Next, a multiconfiguration Hartree-Fock [26] calculation is performed to get the lowest d and f orbitals to describe correlation in the valence shell. Higher n orbitals, which are needed in the R-matrix method, are obtained by constructing a local, screened potential $V_{scr}(r)$ using the HF wave functions of both the inner shells and the valence s and p orbitals. Its explicit form is

$$V_{scr}(r) = -\frac{Z}{r} + \sum_i w_i \int_0^\infty \frac{1}{r_>} P_i^2(r')dr' , \qquad (1)$$

where $r_>$ is the larger of r and r', w_i is the number of electrons in subshell i, and the summation runs over all subshells of the ground configuration of the target ion. Orthogonality with the low-n input orbitals is obtained through the use of Lagrange multipliers in the differential equation. This local potential, which serves to generate orbitals, is not part of the Hamiltonian. The R-matrix method converges fastest when the orbitals are already nearly eigenstates of the Hamiltonian which makes the screening potential of Eq. (1) attractive.

The Hamiltonian, in atomic units, that we use to describe the atom is

$$H = \sum_i H_V(\mathbf{p}_i, \mathbf{r}_i) + \sum_{i<j} 1/r_{ij} - 2\sum_{i<j} P_1(\cos\theta_{ij})\sqrt{V_{pol}(r_i)V_{pol}(r_j)} , \qquad (2)$$

where $\cos\theta_{ij} = \mathbf{r}_i \cdot \mathbf{r}_j / r_i r_j$ and *all* of the atomic electrons are in the Hamiltonian. The one-electron Hamiltonian H_V has the form

$$H_V(\mathbf{p}, \mathbf{r}) = p^2/2 + V_{pol}(r). \qquad (3)$$

The $V_{pol}(r) = -\alpha_d(1 - \exp\{-(r/r_c)^3\})^2/2r^4$ potential is an empirical representation of the interaction of an outer electron with the inner core arising from the core dipole polarizability. The direct inclusion into our basis set of functions that describe this effect would make the calculation prohibitively large. Only in the calculation of Se and Te is the dipole polarizability of the core taken into account. The parameter α_d is taken from Ref. [27] and r_c is determined by evaluating the expectation value $\langle r \rangle$ for orbitals of the outermost closed shell. These parameters are given in Table I.

The calculated energies of the target states are in Table II as an indication of the accuracy of this method.

We will describe the atomic dynamics in the resonance region using ideas based on multichannel scattering theory. We employ the eigenchannel R-matrix procedure to obtain parameters needed to apply multichannel quantum defect theory (MQDT). The variational R-matrix method can be numerically applied in a variety of ways. We use a method given in Ref. [28] which is identical in form to that of Ref. [29]; the Buttle correction of Ref. [28] is not necessary with our choice of basis functions. This R-matrix procedure efficiently obtains a variational estimate of the logarithmic derivative of the wave function at a given energy. Once the wave function and its logarithmic derivative at a given energy are obtained at the R-matrix boundary, the wave function outside the volume is determined by utilizing Coulomb functions; we ignore all electrostatic interactions outside of the R-matrix box. The wave function outside is written in the form

TABLE I. Parameters for constructing the target state wave function. r_0, r_c, and α_d are R-matrix size, range of polarized potential and polarizability of the core, respectively. All numbers are in a.u.

	Parameters		
Atom	r_0	r_c	α_d
O	11.0		0.0
S	13.0		0.0
Se	13.0	0.6	0.3604
Te	13.0	0.9	1.295

$$\psi_i = \mathcal{A} \sum_j \Phi_j^{(LS)}(\Omega)[f_j(r)\delta_{ji} - g_j(r)K_{ji}^{(LS)}], \quad (4)$$

where $\mathcal{A}$ is the antisymmetrization operator, $\Phi_j^{(LS)}(\Omega)$ is the target wave function, $f_j(r)$ and $g_j(r)$ are regular and irregular Coulomb functions for channel j, respectively, and $K_{ji}^{(LS)}$ is the reaction matrix. This K matrix and the reduced dipole matrix elements $d_i = \langle \psi_i || D || \Psi_o \rangle$ are the only parameters needed to obtain the photoabsorption cross section.

Because the target state has a half-filled p shell, the number of different angular couplings for a close-coupling basis is enormous. To keep our calculation to a reasonable size only five configurations for the target states are chosen. The rare gas core electrons are frozen; we do not include any correlation or virtual excitations of inner core electrons. The discussion of configurations that follows refers to the valence electrons. For every shell configuration (e.g., $3s3p^3 3d4d$) included in the calculation, all possible intermediate angular couplings are included. Both open- and closed-type bases are used if the $LS\pi$ term of the $N-1$ electron target state can interact with the ns^2np^3 target states while only closed-type bases are used for all other configurations. (Closed-type basis is a wave function that vanishes at the R-matrix boundary while open type does not.) The open-type basis functions in this calculation have zero derivative at the boundary. Table III summarizes the configurations and their mixing coefficients for the target states of sulfur. We use the same configuration lists for the different atoms and do not reoptimize the configuration list for different atoms. The only difference between the atoms is the radial orbitals of the valence electrons and the electrons in the inner closed shells.

TABLE II. The calculated and experimental energies of target states relative to $^4S^o$.

		Energy (a.u.)	
Atom	State	Present	Experiment[a]
O	$^2D^o$	0.12807	0.12219
	$^2P^o$	0.19678	0.18438
S	$^2D^o$	0.07350	0.06776
	$^2P^o$	0.12025	0.11189
Se	$^2D^o$	0.06660	0.06168
	$^2P^o$	0.11408	0.10757
Te	$^2D^o$	0.05513	0.05259
	$^2P^o$	0.09785	0.10421

[a]Reference [32].

The spin-orbit interaction is approximately included in the calculation through the LS-jj frame transformation [30]. The energy splitting of the target state of Se is $\sim$ 800 cm^{-1}. For Te, the energy splitting for $^2D^o$ is 2201 cm^{-1} and for $^2P^o$ is 3487 cm^{-1}. The frame transformation works well when the quantum defects do not vary over energy ranges comparable to the spin-orbit splitting of the threshold and when the spin-orbit interaction of a Rydberg electron is much smaller than that of the target state. The frame transformation has worked well in the photoionization spectrum of Ba which has spin-orbit splittings of 1690.9 cm^{-1}. Because the transformation does not consider the dynamics of the mixing between states with the same total angular momentum but dif-

TABLE III. Configurations and their mixing coefficients for the target states of atomic sulfur.

$3s^23p^3\ ^4S^o$	$3s^23p^3$	$3s3p^33d$	$3s^23p3d^2$		
	0.977	0.194	0.091		
$3s^23p^3\ ^2D^o$	$2s^23p^3$	$3s3p^3(^4S^o)[^3S^o]3d$	$3s3p^3(^2P^o)[^1P^o]3d$	$3s3p^3(^2P^o)[^3P^o]3d$	$3s3p^3(^2D^o)[^1D^o]3d$
	0.973	0.114	0.001	−0.014	−0.133
	$3s3p^3(^2D^o)[^3D^o]3d$	$3s^23p3d^2(^3P)$	$3s^23p3d^2(^1D)$	$3s^23p3d^2(^3F)$	$3s^23p^2(^3P)4f$
	0.083	−0.064	0.083	−0.009	0.058
	$3s^23p^2(^1D)4f$				
	0.044				
$3s^23p^3\ ^2P^o$	$2s^23p^3$	$3s3p^3(^2P^o)[^1P^o]3d$	$3s3p^3(^2P^o)[^3P^o]3d$	$3s3p^3(^2D^o)[^1D^o]3d$	$3s3p^3(^2D^o)[^3D^o]3d$
	0.963	0.104	−0.079	0.014	0.049
	$3s^23p3d^2(^1S)$	$3s^23p3d^2(^3P)$	$3s^23p3d^2(^1D)$	$3s^23p^24f$	$3p^5$
	0.123	−0.064	−0.074	−0.041	0.164

ferent total spin or orbital angular momentum, it may fail to give good results for Te. The striking success of the frame transformation for Ba may be due to the fact that the spin-orbit interaction cannot mix ionic states of different parity.

The photoionization cross section is approximated by the photoabsorption cross section in this calculation. They are nearly identical if the branching ratio for autoionization versus radiative emission is large. To compare the calculated cross section to the experiment with finite resolution a preconvolved technique [31] is used. This method utilizes the same parameters in the calculation of an infinite resolution photoabsorption cross section to obtain the cross section at a certain energy that has been convolved over a width Γ. The resolution of the experiment full width at half maximum is used as the width in the calculations.

IV. RESULTS AND DISCUSSION

We concentrate our calculations in the energy region between the first and the third ionization thresholds ($^4S^o$ and $^2P^o$, respectively). The threshold energies are taken from Ref. [32] and are necessary for the MQDT part of the calculation. All of the calculations are from the $ns^2np^4\ ^3P_2$ ground state of the neutral atoms.

A. Oxygen

There is a similarity between the spectrum of the chalcogens and that of the halogens, namely, the absence of broad features in the second row elements (O and F). This is a consequence of small overlap between $2p$ and nd orbitals in these elements as mentioned in Ref. [24]. The d waves cannot penetrate the angular momentum barrier and interact strongly with the electrons of the valence shell. Because the d waves interact weakly with the valence electrons, they cannot quickly exchange energy with the core and autoionize.

Figures 1 and 2 show the experimental photoionization and theoretical photoabsorption cross section of O between the $^4S^o$ and $^2P^o$ threshold. In the experiment there are satellite absorptions from the $2s^22p^4\ ^3P_{1,0}$ states which are not included in our calculation. The first intense peak at $\sim$ 872 Å is $(^2P^o)3s\ ^3P^o$. This LS forbidden state is the lowest Rydberg state attached to the $^2P^o$ threshold and the position is off by about 6 Å. This large wavelength error is due to the small effective quantum number of this state; the error in the energy is equal to the error in the quantum defect divided by the effective quantum number cubed. In terms of quantum defect the error is 0.020. The intense peak $2s2p^5\ ^3P^o$ at $\sim$ 787 Å causes some troubles in the calculation. We have shifted the position of this peak to its experimental position because the size and shapes of other $^3P^o$ resonances were sensitive to its position. The height of the resonance at $\sim$ 811 Å decreases by a factor of 4 when the $2s2p^5$ is unshifted. The error in the position of the $2s2p^5$ resonance was 4.5 Å. The error in the energy of this state is not surprising because we use the ionic one-electron wave functions as basis functions. The $2s$ and $2p$ orbitals are closer to the nucleus than in the case of neutral oxygen and, therefore, push the $2s2p^5$ state too high in energy. The oxygen cross section with the shifted peak is shown in Fig. 1.

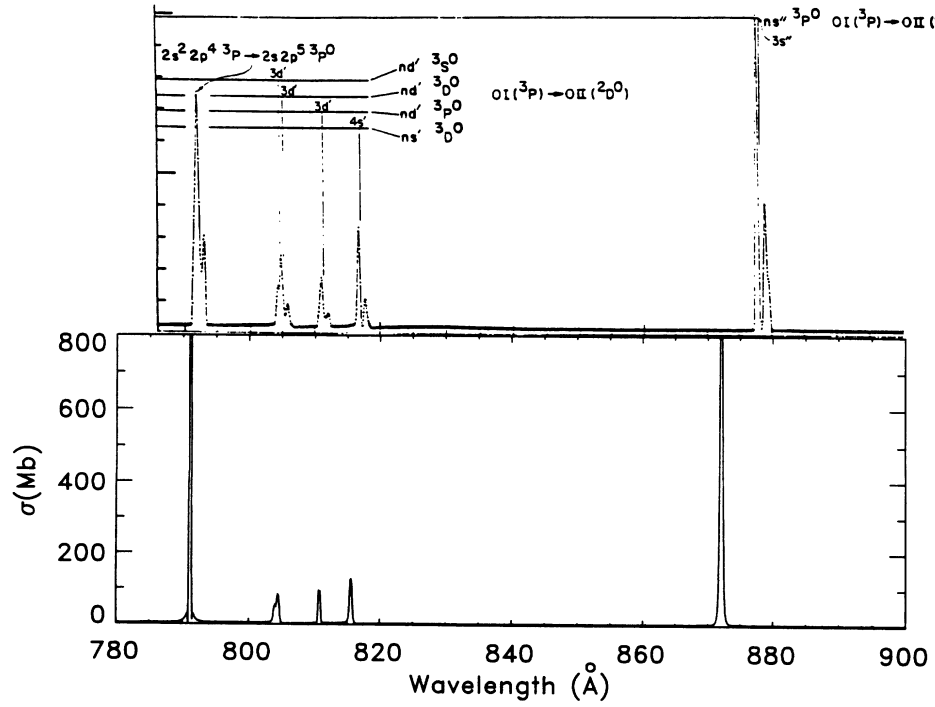

FIG. 1. Theoretical photoabsorption (lower) and experimental photoionization (upper) cross section of O between the $^4S^o$ and $^2D^o$ thresholds. The position of the $2s2p^5$ state at $\sim$ 792 has been shifted to the experimental energy. The preconvolved cross section is calculated with width Γ = 0.000 32 a.u.

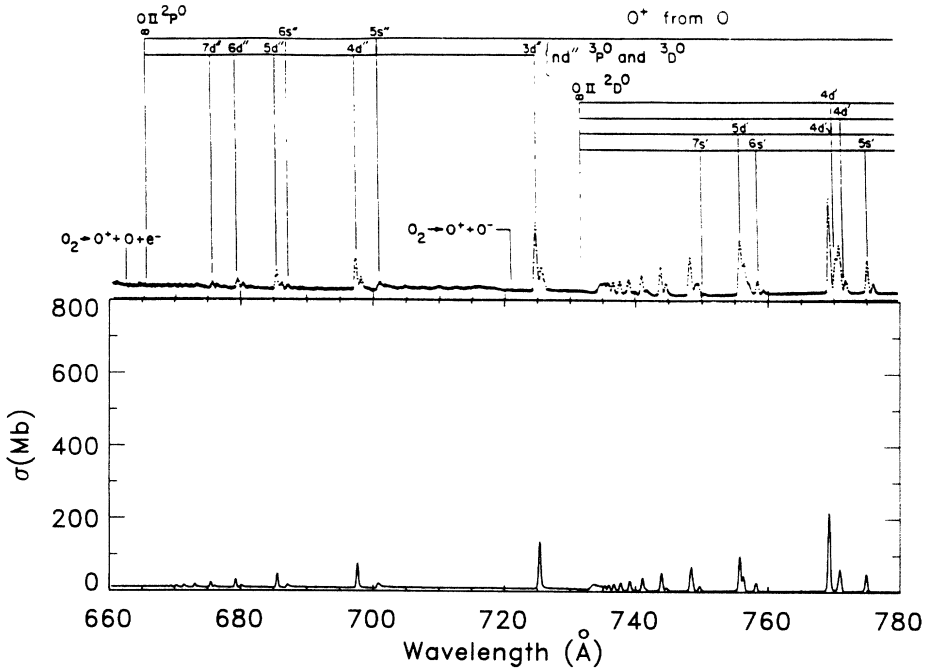

FIG. 2. Same as Fig. 1 but between the $^2D^o$ and $^2P^o$ thresholds.

B. Sulfur

The experimental photoionization cross section of S shows both broad and sharp features. Between the $^4S^o$ and $^2D^o$ thresholds the broad resonance is $(^2D^o)nd\,^3D^o$ and the sharp ones are $(^2D^o)nd\,^3S^o$, $(^2D^o)ns\,^3D^o$, and $(^2D^o)nd\,^3P^o$. The $^2D^o$ and $^2P^o$ target states have very small splittings; all of the resonances seen in the experiment are classified best in LS coupling. The $^3P^o$ final state is LS forbidden in this energy range but we include these channels in our calculation assuming that the Rydberg states decay by autoionization due to the weak spin-orbit interaction. These states are weakly coupled to the open channels and, therefore, they are very narrow in the spectrum. Figure 3 shows the experimental photoionization and the calculated photoabsorption cross section in this energy range. The calculated cross section of $(^2D^o)3d\,^3P^o$ at 1156 Å is too big by a factor of 10. As the overall spectrum agrees well with the experiment, this discrepancy indicates to us that the $(^2D^o)3d\,^3P$ states

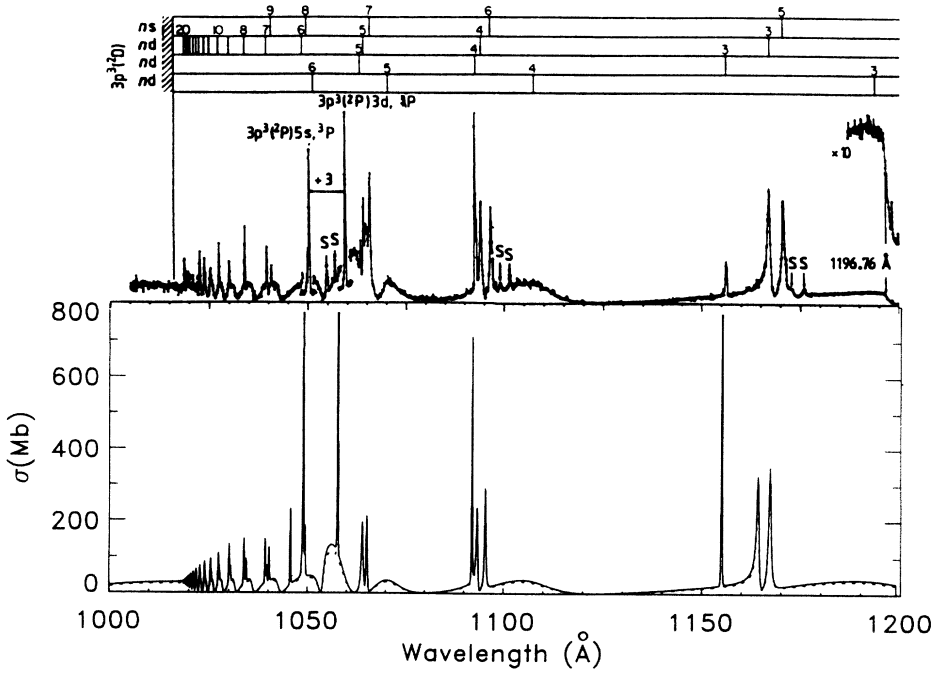

FIG. 3. Theoretical photoabsorption (lower) and experimental photoionization (upper) cross section of S between the $^4S^o$ and $^2D^o$ thresholds. The preconvolved cross section is calculated with width Γ = 0.0001 a.u. The resonances at 1156 Å, 1059 Å, and 1050 Å have calculated heights of 990 Mb, 1160 Mb, and 1410 Mb.

decay more rapidly by photon emission. To estimate the lifetime of this state, we have performed calculations using the LS-jj frame transformation to approximately include the spin-orbit interaction that allows this state to decay. This resonance splits into two peaks in the spectrum as the result of the fine structure. We obtain a width of $\sim 10^{-7}$ a.u. which corresponds to a lifetime of $\sim 10^{-10}$ s. This calculation would indicate that this state decays by autoionization. However, this is an extremely long lifetime (for a $3d$ autoionizing state) which is nearly comparable to decay times by photon emission. It is a strong possibility that the autoionization rate would decrease in a calculation that included the full spin-orbit effect.

There has been some questions about the assignment of the $(^2D^o)ns\,^3D^o$ and $(^2D^o)nd\,^3S^o$ series. Our calculation suggests that the assignment of these series from the experiment should be reversed from that of Ref. [17]. The resonance peak at longer wavelength is always $(^2D^o)nd\,^3S^o$. Some of the evidence for our classification involves the derivatives of the quantum defects with respect to energy. Our classification of these two series agrees with Tayal [15]. The comparison of this classification and others are shown in Table IV. For most resonances the errors of quantum defects are within 0.02.

Near the $^2D^o$ threshold there is no perturber and the quantum defects of nearby high Rydberg states are nearly energy independent in our calculation. The experiment shows, however, an irregular energy dependence of the quantum defects. As a series approaches its limit, the quantum defect depends sensitively on its position relative to the limit. For $n \sim 16$, a 0.01-Å error in the experimental position of a resonance causes an error of 0.02 in the quantum defect.

There are three perturbers attached to the $^2P^o$ threshold that lie in the energy range between 1150 Å–1160 Å. The broad resonance is $(^2P^o)3d\,^3D^o$ and the two sharp ones are $(^2P^o)3d\,^3P^o$ and $(^2P^o)5s\,^3P^o$. The two $^3P^o$ resonances are forbidden to decay in LS coupling which is why they are sharp. The errors of the quantum defects of these states are ~ 0.015. They are all far away from the $^2P^o$ threshold and this calculation does not give the correct shape of the broad resonance. Especially, the $(^2P^o)5s\,^3P^o$ state affects the nearby $(^2D^o)6d\,^3P^o$ state and produces a prominent peak at 1045 Å . Figure 4 shows the cross section between $^2D^o$ and $^2P^o$ thresholds. The agreement is quite satisfactory. However, the calculated $(^2P^o)nd\,^3P^o$, $^3D^o$ series are broad and overlapping. It is not possible to distinguish them in the total cross section. The classification in Table V is made based on the partial cross sections. All previous calculations of the total cross section seem to give good agreement in this energy range.

Recent calculations of S by Tayal [15] and by Altun [21] gave global agreements with the experiment but some of the resonances had an error greater than 0.1 in the quantum defect. An error of this order not only shifts the position of the sharp resonances but also changes the shape of the broad resonances. The cross section of Ref. [21] near the $^2D^o$ threshold region did not agree with experiment, especially the $(^2D^o)3d\,^3D^o$ broad resonance did not seem to appear. They attributed the discrepancies to the approximations of the target states and the omission of the spin-orbit interaction. As we also neglect the spin-

TABLE IV. Position and classification of autoionizing series of atomic sulfur converging to $^2D^o$ threshold.

	Position (Å)					Quantum defect μ				
	Present	Gibson *et al.*[c]	Tayal[a]	Altun[b]	Mendoza and Zeippen[d]	Present	Gibson *et al.*[c]	Tayal[a]	Altun[b]	Mendoza and Zeippen[d]
$3s^2 3p^3(^2D^o)5s\,^3D^o$	1164.4	1167.2[e]	1145.5	1165.8	1166.3	2.043	2.067[e]	1.861	2.055	2.059
$6s\,^3D^o$	1093.5	1094.3[e]	1086.8	1109.7	1093.7	2.036	2.054[e]	1.863	2.367	2.039
$7s\,^3D^o$	1064.2	1064.0[e]	1060.8	1064.2	1064.0	2.043	2.031[e]	1.869	2.044	2.034
$8s\,^3D^o$	1048.6	1048.5[e]	1048.4	1048.9		2.020	2.007[e]	1.996	2.039	
$9s\,^3D^o$	1039.8	1039.4[e]				2.022	1.970[e]			
$3s^2 3p^3(^2D^o)3d\,^3S^o$	1167.2	1170.5[e]	1163.0	1193.9	1166.7	0.067	0.094[e]	0.031	0.265	0.063
$4d\,^3S^o$	1095.5	1096.6[e]	1093.9	1100.4	1095.6	0.081	0.107[e]	0.044	0.189	0.083
$5d\,^3S^o$	1065.2	1065.8[e]	1064.4	1066.1	1065.1	0.088	0.118[e]	0.050	0.131	0.085
$6d\,^3S^o$	1049.5	1049.7[e]	1049.0	1049.4	1049.4	0.092	0.111[e]	0.054	0.085	0.084
$7d\,^3S^o$	1040.3	1040.6[e]	1040.0	1039.6		0.095	0.140[e]	0.056	0.002	
$8d\,^3S^o$	1034.4	1033.9	1035.6	1034.0		0.096	-0.013	0.327	0.005	
$9d\,^3S^o$	1030.4	1029.9				0.097	-0.072			
$10d\,^3S^o$	1027.6	1027.3				0.098	-0.045			
$11d\,^3S^o$	1025.6	1025.3				0.099	-0.056			
$12d\,^3S^o$	1024.0	1023.7				0.099	-0.135			
$13d\,^3S^o$	1022.8	1022.5				0.100	-0.192			
$14d\,^3S^o$	1021.8	1021.8				0.100	0.046			
$3s^2 3p^3(^2D^o)3d\,^3P^o$	1155.0	1156.3				-0.043	-0.034			
		1156.0								
$4d\,^3P^o$	1092.1	1092.7				0.001	0.016			
$5d\,^3P^o$	1065.4	1063.3				0.098	-0.004			

[a]Reference [15].
[b]Reference [21].
[c]Reference [17].
[d]Reference [20].
[e]Switch the assignment of $(^2D^o)ns\,^3D^o$ and $(^2D^o)(n-2)d\,^3S^o$ from Gibson *et al.* [17].

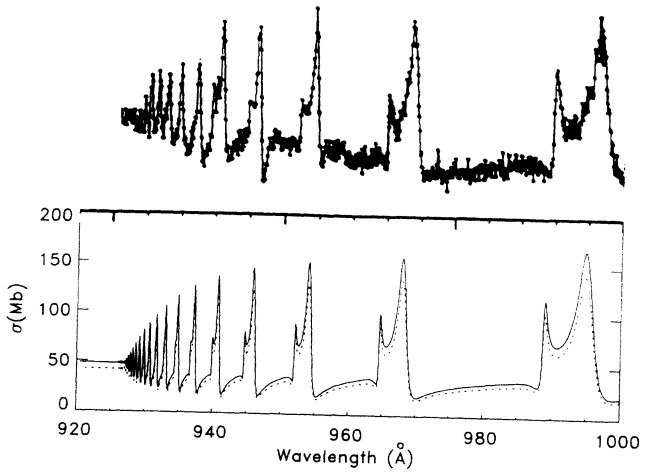

FIG. 4. Same as Fig. 3 but between the $^2D^o$ and $^2P^o$ thresholds.

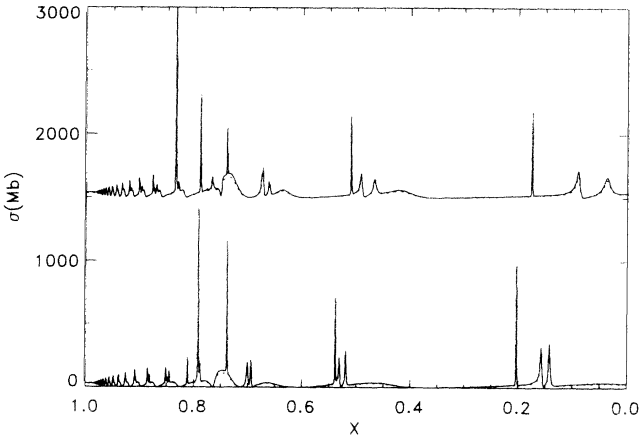

FIG. 5. Photoionization cross sections of S (lower) and Se (upper by +1500) in LS coupling versus a dimensionless quantity $x = (\omega - E_{^4S^o})/(E_{^2D^o} - E_{^4S^o})$.

orbit interaction and keep only five configurations for the ionic states, we do not think this can be the explanation.

C. Selenium

We have calculated the photoionization cross section of S using the frame transformation to incorporate the spin-orbit interaction and the result did not significantly change as compared to an LS calculation. However, in Se the spin-orbit splitting of the thresholds is a factor of 20 larger than S and the frame transformation significantly changes the cross section. Nevertheless, some resemblances to S can be found in the Se spectrum near the first threshold but at higher n there does not appear to be any resemblance. To reveal the similarities between S and Se, we plot the S and the Se spectra in LS coupling on the same scale. Figure 5 clearly shows the similarities between the two atoms. They also have the same ordering of the two sharp series from $^3S^o$ and $^3D^o$. From this comparison it is obvious that the two atoms have nearly identical electrostatic interactions between the valence and the Rydberg electron. It is the spin-orbit interaction, which increases with nuclear charge, that destroys the similarity between the atoms.

Figure 6 shows the cross section in jj coupling between

TABLE V. Position and classification of autoionizing series of atomic sulfur converging to $^2P^o$ threshold.

	Position (Å)					Quantum defect μ				
	Present	Gibson *et al.*[c]	Tayal[a]	Altun[b]	Mendoza and Zeippen[d]	Present	Gibson *et al.* [c]	Tayal[a]	Altun[b]	Mendoza and Zeippen[d]
$3s^23p^3(^2P^o)5s\,^3P^o$	1049.0	1050.2			1039.1	2.070	2.085			1.962
		1050.4								
$6s\,^3P^o$	989.0	990.0	983.0	989.9	988.9	2.041	2.170	1.855	2.067	2.040
$7s\,^3P^o$	964.7	965.0	961.8	965.1	964.7	2.035	2.056	1.854	2.061	2.035
$8s\,^3P^o$	952.1	952.3	950.5	952.2	952.1	2.033	2.056	1.856	2.046	2.032
$9s\,^3P^o$	944.7	944.9	943.7	944.6		2.031	2.070	1.859	2.026	
$10s\,^3P^o$	940.0	940.1	939.4	937.9		2.030	2.068	1.874	1.419	
$3s^23p^3(^2P^o)3d\,^3P^o$	1057.7	1059.5			1048.5	0.157	0.173			0.064
$4d\,^3P^o$	995.2	996.5	992.5	997.1	997.1	0.209	0.241	0.139	0.254	0.254
$5d\,^3P^o$	968.2	968.6	966.9	967.1	968.9	0.235	0.255	0.163	0.176	0.270
$6d\,^3P^o$	954.2	954.3	953.5	953.8	954.5	0.248	0.257	0.176	0.209	0.276
$7d\,^3P^o$	946.0	946.3	945.6	945.6		0.256	0.295	0.187	0.183	
$8d\,^3P^o$	940.9	941.0	940.6	940.7		0.262	0.290	0.190	0.220	
$3s^23p^3(^2P^o)4d\,^3D^o$	994.8	994.6	992.5	996.7	992.9	0.198	0.193	0.138	0.245	0.149
$5d\,^3D^o$	967.9	967.4	966.7	967.8	966.8	0.219	0.191	0.155	0.213	0.160
$6d\,^3D^o$	954.0	953.6	953.4	954.5	953.4	0.231	0.189	0.166	0.273	0.162
$7d\,^3D^o$	945.9	945.7	945.5	945.4	945.4	0.237	0.201	0.173	0.148	0.161
$8d\,^3D^o$	940.8	940.6	940.5	940.6		0.241	0.194	0.174	0.185	
$9d\,^3D^o$	937.3	937.2				0.244	0.194			
$10d\,^3D^o$	934.9	934.8				0.246	0.193			

[a]Reference [15].
[b]Reference [21].
[c]Reference [17].
[d]Reference [20].

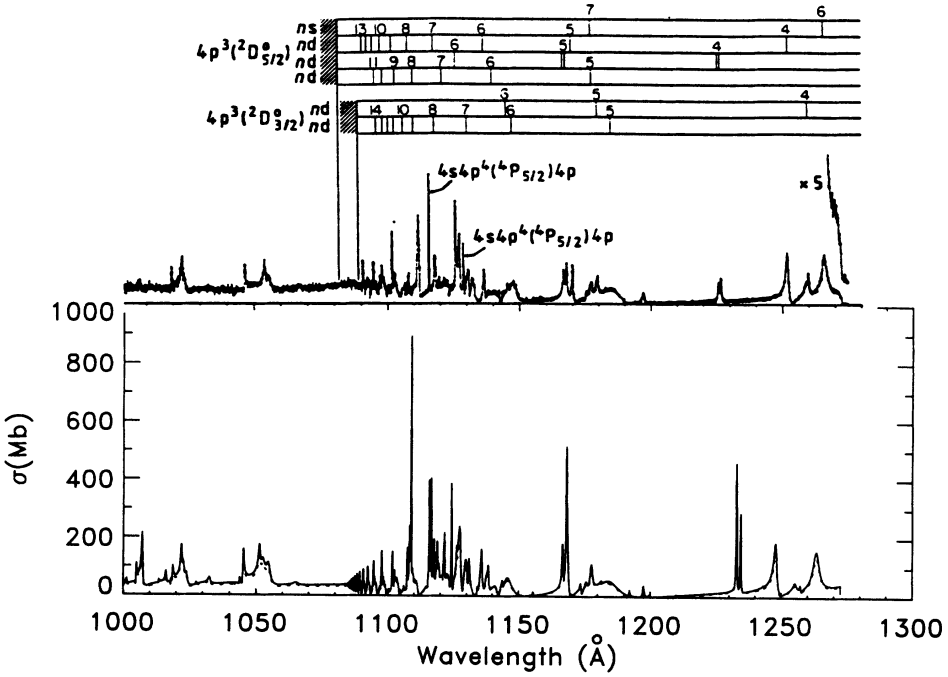

FIG. 6. Theoretical photoabsorption (lower) and experimental photoionization (upper) cross section of Se. The preconvolved width Γ is 0.0001 a.u.

threshold and 1000 Å. The calculated results below $^2D^o$ give global, but not detailed, agreement with the experiment. However, there are several energy ranges where the agreement with experiment is remarkably good and, in fact, most of the discrepancies are near the perturbers at ~ 1120 Å attached to the $^2P^o$ threshold. Most of the resonance states are strongly mixed and make the classification quite difficult. However we still can assign the lowest resonance to be $(^2D^o)4d\ ^3S^o_1$ at 1265.9 Å and the error of the calculated quantum defect $\Delta\mu$ is ~ 0.018. The resonance at 1251.9 Å is $(^2D^o)6s\ ^3D^o_3$ with $\Delta\mu$ ~ 0.030. Two sharp peaks much higher than the experiment at ~ 1226 Å are from $^3P^o$ final state. The widths are ~ 10^{-5} a.u. Their positions are too low by ~ 7 Å. The lower resonance is $(^2D^o)4d\ ^3P^o_1$ at 1226.5 Å with $\Delta\mu$ ~ 0.077 and the higher one is $(^2D^o)4d\ ^3P^o_2$ at 1225.7 Å with $\Delta\mu$ ~ 0.070. A small peak at 1197.7 Å is almost identical to a peak in the experiment although it was not classified in the experiment. We assign it as $^3F^o_3$. The next group is similar to the spectrum of S. The broad resonance is $(^2D^o)5d\ ^3D^o_3$ at ~ 1185 Å. The sharp one is $(^2D^o)5d\ ^3S^o_1$ at 1179.6 Å. From the similarities between S and Se it is not surprising that Se has the same ordering of $(^2D^o)nd\ ^3S^o$ and $(^2D^o)ns\ ^3D^o$ resonances as S. Our assignment of the $(^2D^o)nd\ ^3S^o$ and $(^2D^o)ns\ ^3D^o$ resonances reverses the classification from the experiment.

There are two peaks assigned by the experiment as $4s4p^4(^4P_{5/2})4p$ states. We have used a large basis set and diagonalized the Hamiltonian to find the position of the $4s4p^5$ state. We found the $4s4p^5$ state was mixed with many states over an energy range of ~ 7 eV. The maximum weight for the $4s4p^5$ state is only 23% and is below threshold. The states near 1120 Å only have a few percent admixture of $4s4p^5$. The $4s4p^5$ state should not be assigned to any of the experimental resonances. However, the states that are classified $4s4p^5$ in the experiment are clearly perturber states because the $(^2D^o)nl$ Rydberg series are irregular near that energy. These perturbers are analogous to the ones in S and can be classified as $(^2P^o)6s\ ^3P^o$ and $(^2P^o)4d\ ^3P^o$.

Above the $^2D^o$ threshold only two groups of resonance states are found in the experiment. In the calculation, the Rydberg states converging to $^2P^o$ are still clear to much higher n. This discrepancy with experiment will be discussed in more detail in the section on Te.

Although the agreement of Se is not as good as S, this calculation shows the frame transformation is a good approximation for Se. Most of the disagreement with experiment is near the perturbers at 1120 Å; these sorts of problems are very difficult to overcome because a small error in the positions of perturbers has a large effect on the cross section.

D. Tellurium

The cross section of Te is shown in Figs. 7 and 8. It is clear that the quality of the calculation has decreased over that of Se. The reason for the inaccuracy cannot be definitely ascertained. It is possible that the main errors enter the calculation through the approximate method (LS-jj frame transformation) for including the spin-orbit interaction. It may be necessary to include relativistic effects while the electron is inside the R-matrix box. Or it may be necessary to include the coupling of the ionic states through the spin-orbit interaction (e.g., the ns^2np^3 $^2P^o_{3/2}$, $^2D^o_{3/2}$, and $^4S^o_{3/2}$ states mix through the spin-orbit interaction). Another possibility is that the wave functions might not be converged for Te. The polarizability of Te^+ is larger than that of Se^+ which may indicate that

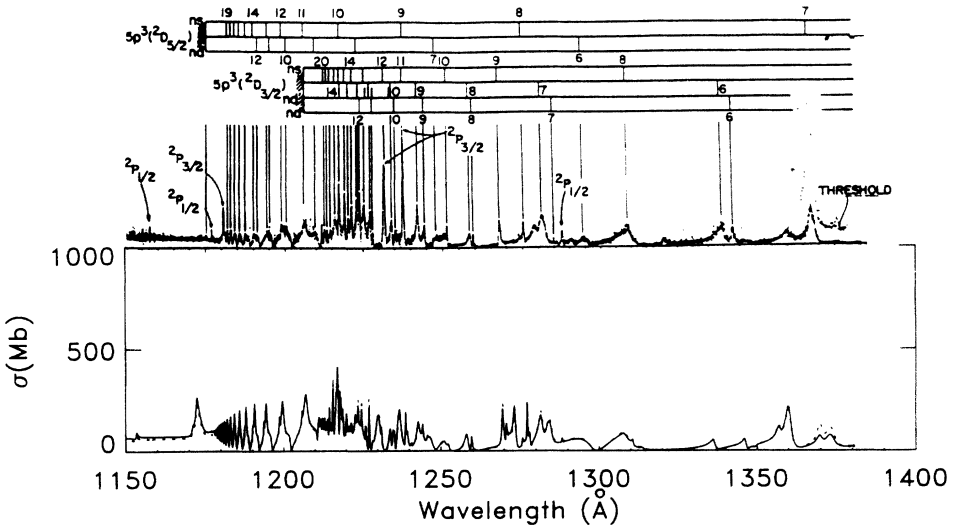

FIG. 7. Theoretical photoabsorption (lower) and experimental photoionization (upper) cross section of Te below $^2D^o$ threshold. The preconvolved width Γ is 0.00008 a.u.

correlations are more important.

The resonances are more strongly mixed in Te than in Se. Some of them, which are similar to the experiment, can be identified. At 1342.98 Å is $(^2D^o_{3/2}6d)_{J=3}$ and at 1339.48 Å is $(^2D^o_{3/2}6d)_{J=3}$. $(^2D^o_{3/2}8s)_{J=2}$ at 1308.92 Å appears to be relatively broad. Near 1260 Å are $(^2D^o_{3/2}8d)_{J=3}$ at 1259.58 Å and $(^2D^o_{3/2}8d)_{J=3}$ at 1158.40 Å. Above $^2D^o$ we have well matched resonances such as $(^2P^o_{1/2}8d)_{J=3}$ at 1114.85 Å, $(^2P^o_{3/2}8s)_{J=2}$ at 1112.10 Å, $(^2P^o_{1/2}9d)_{J=3}$ at 1102.00 Å , and $(^2P^o_{3/2}8d)_{J=2}$ at 1071.48 Å. However, we assign the resonance at 1131.15 Å to be $(^2P^o nd)\ ^3F_3$ and the one at 1128.00 Å to be $(^2P^o_{1/2}9s)_{J=1}$.

The experimental and theoretical cross sections do not correspond very well between the $^2D^o$ and $^2P^o$ thresholds for both Se and Te. While the calculations are far from perfect, we have reason to believe the experimental cross section is not as accurate in this energy range as it is between the $^4S^o$ and $^2D^o$ thresholds. One problem with the experiment is missing Rydberg resonances. (This problem was also noted for Rydberg series between the $ns^2np^4\ ^1D$ and ^1S thresholds in Br and I [24].) In the calculation, the low-n Rydberg states have roughly the same height as higher-n states whereas the experimental resonances rapidly decrease with n. Since a characteristic of unperturbed Rydberg series is their slow evolution with n, we feel that the experiments are probably not measuring the cross section of the atom in this energy range. We do not have any ideas about the cause of the discrepancy.

In Te, there are possible experimental problems between 1035 Å and 1065 Å . In this range there are a large number of sharp peaks, some of which have a very

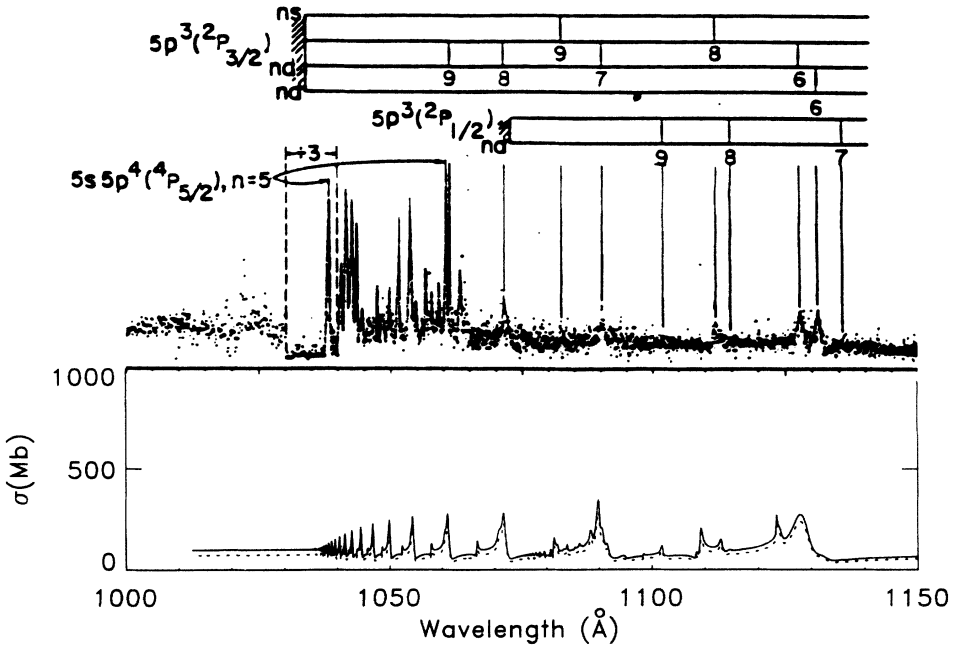

FIG. 8. Same as Fig. 7 but between the $^2D^o$ and $^2P^o$ thresholds.

small energy spacing. In the experiment, some of the peaks were identified as $5s5p^5$ resonances. None of the structures correspond to features in the calculation. We used a very large configuration interaction calculation of the $5s5p^5$ states, and we found them to be very strongly mixed with the $5s^25p^3nd, \varepsilon d$ states and continua. We found the $5s5p^5$ states to have an energy width of ~ 5 eV (see the discussion above about the $4s4p^5$ states in Se). For this reason, we do not accept the classification given in the experiment. The next threshold above the $^2P^o$ threshold is the $5s5p^4\ ^4P$ which is ~ 0.22 a.u. higher in energy than the $^2P^o$ threshold. If the perturbers near 1050 Å are attached to this threshold, they would have an effective quantum number of ~ 1.5 which is too small by ~ 1.5. Similar considerations eliminate perturbers attached to all higher thresholds. Having ruled out the $5s5p^5$ states, we cannot find any possible perturber that would fall near this energy. Another problem with the experimental spectrum is that the closely spaced resonances do not have the proper Rydberg spacing for $^2P^o_{3/2}nl$ states. For these reasons, we feel that many of the experimental resonances do not correspond to resonances in atomic Te and are possibly due to impurities in the vapor.

V. ORIGIN OF SPECTRAL FEATURES

In this section, we examine the generic physics of S in some detail. This enables us to show how various features in the spectrum arise.

A. Convergence of wave function

The wave functions of multielectron atoms cannot be determined exactly. A goal of the calculation is to approximate the wave function with as few functions as possible. To reach this goal, it is desirable to know what sort of effects are important. To this end, we have performed several calculations with different basis sets starting from HF functions to our final calculation with several hundred basis. In Table VI we present the quantum defect μ of the lowest five Rydberg states from the calculation on $^3S^o$ of sulfur. We have switched the classification of $^3S^o$ and $^3D^o$ of the experimental quantum defects cited in this table based on the evidence of the full calculation.

This calculation serves to demonstrate how a certain basis affects the positions of the autoionization resonances. A simple HF calculation gives errors of ~ 0.08 in the quantum defect compared to the experiment. This shows the HF calculation does not include the physical effect that determines the d-wave quantum defect in S. Adding correlation-type configurations to the core state gives ~ 0.1 error. The reason for this worse result is that including the correlation effect helps to converge the core state more than the Rydberg state and, therefore, lowers the $^2D^o$ threshold compared to the positions of the resonances. (It might be argued from this that it is better to neglect correlation. However, the positions of the resonances are just one aspect of the spectrum. A better description of the target state is essential to channel interactions and to dipole matrix elements and should not be sacrificed.)

The type of basis functions that converge the quantum defect the best for d-wave Rydberg states are those that represent dipole polarization of the valence shell. These basis functions have even parity of the core with odd parity of the outer electron (e.g., $3s^23p^23dnf$ functions help converge the $3s^23p^3nd$ states). The quantum defects are changed by ~ 0.07 when these basis functions are added. This calculation shows the polarization-type configurations play a key role in converging the final state wave function and should be included in the calculation.

To include the effect of polarization of the $3p$ shell, we used the $3d$ orbital calculated from the correlation of the $3p$ shell. Calculations that use spectroscopic $3d$ orbitals instead of the correlation orbital grossly underestimate the polarization of the $3p$ shell. We calculated the resonance positions using a polarized $3d$ orbital [33]. The quantum defect changed by too large an amount when the polarized $3d$ orbital was used. The error in the quantum defect was larger with the polarized $3d$ orbital than with the correlation $3d$ orbital for the same configuration list. The reason for the over correction is the polarized $3d$ orbital does not represent correlation of the target state very well, which raises the threshold energy relative to the Rydberg state energy. A basis set that included the correlated $3d$ orbital for the target state and the polarized $3d$ orbital for the polarization basis functions would be optimal but is beyond the scope of our programs.

B. Model potentials

In the past, calculations on complicated atomic systems have included a model potential to account for the effect of closed shells common to all states (e.g., see Ref. [34] for the method of determining the model potential). This approximation is intuitively sensible when there are few valence electrons. However, the approximation becomes somewhat problematical for a large number of valence electrons and it is somewhat worrisome that the approximation cannot be improved systematically. Because of these worries, we have modified our R-matrix programs to incorporate multiconfiguration HF orbitals. This addition allowed us to do parallel calculations with the same configuration list with one calculation using 16 electrons and the other calculation using a model potential and 6 electrons. For all levels of complication of basis sets and for all symmetries, the quantum defects of the parallel calculations differed by less than 0.01. The dipole matrix elements also contained negligible differences. This shows the Ne-like core can be well approximated with a local potential. This is because most of the interesting channel coupling arises from the interaction of the Rydberg electron with the valence electron. For the heavier alkaline earths (Ca, Sr, and Ba), it was necessary to use a model potential to obtain agreement with experiment due to the sensitivity of the d waves to the screening potential. This does not seem to be the case for the chalcogens.

C. General spectral trends

It is very gratifying to obtain good agreement of the calculations with experiment. However, the good agreement comes at the expense of a very large calculation. The size of the calculation tends to obscure the simple origin of many features of the spectrum. Several of the most noticeable features are already present in simple calculations using Hartree-Fock target states. At this level of approximation it is sufficient to examine the matrix elements of the $1/r_{ij}$ operator to find the couplings between channels and the relative energies of the Rydberg states because the one-electron operators do not depend on the angular momentum couplings between electrons. As the prototype atom we examined the matrix elements for S.

To get a better understanding about the origin of the broad and sharp features of the S spectrum, we have analyzed the off-diagonal matrix elements of the $1/r_{ij}$ interaction between different channels. At the perturbative level, the width of the resonance is proportional to the square of the off-diagonal $1/r_{ij}$ matrix elements; a small off-diagonal matrix element indicates a sharp resonance and a large off-diagonal matrix element indicates a broad resonance. For the purposes of estimating the coupling, a near zero energy $7s$ and a $5d$ orbital are created by choosing an appropriate box size to emulate threshold electrons. These orbitals should be adequate for estimating the radial matrix elements involving Rydberg electrons or near zero energy continuum electrons. The matrix element of $1/r_{ij}$ between $3s^23p^3(^4S^o)5d\ ^3D^o$ and $3s^23p^3(^2D^o)5d\ ^3D^o$ is five times bigger than that between $3s^23p^3(^4S^o)5d\ ^3D^o$ and $3s^23p^3(^2D^o)7s\ ^3D^o$. This means the coupling of $(^2D^o)nd$ and the open channel is greater than that of $(^2D^o)ns$ and the open channel, therefore, the nd resonances are broader than the ns resonances. The $1/r_{ij}$ matrix element between the $3s^23p^3(^4S^o)7s\ ^3S^o$ and the $3s^23p^3(^2D^o)5d\ ^3S^o$ states is ~ 2.3 times smaller than that between the $(^4S^o)5d\ ^3D^o$ state and the $(^2D^o)5d\ ^3D^o$ state. These matrix elements correctly describe the general trend of the spectrum, i.e., broad $(^2D^o)nd\ ^3D^o$ states and sharp $(^2D^o)ns\ ^3D^o$ and $(^2D^o)nd\ ^3S^o$ states.

The reason for the relative sizes of these matrix elements can be understood from simple arguments. First, the only nonzero terms in the $1/r_{ij}$ interaction are exchange terms involving the open p shell because the spin of the core changes in the interaction, i.e., $(^2D^o)nl \rightarrow (^4S^o)\varepsilon l'$. This means that for the coupling between the $(^2D^o)nd\ ^3D^o$ and $(^4S^o)\varepsilon d\ ^3D^o$ continuum the $3p \rightarrow \varepsilon d$ and the $nd \rightarrow 3p$, for the coupling between the $(^2D^o)ns\ ^3D^o$ states and the $(^4S^o)\varepsilon d\ ^3D^o$ continuum the $3p \rightarrow \varepsilon d$ and the $ns \rightarrow 3p$, and for the coupling between the $(^2D^o)nd\ ^3S^o$ states and the $(^4S^o)\varepsilon s\ ^3S^o$ continuum $3p \rightarrow \varepsilon s$ and $nd \rightarrow 3p$. By the propensity rule for exciting and deexciting orbitals, when an electron gains energy it also tends to gain angular momentum and when an electron loses energy it prefers to lose angular momentum. Therefore, the transitions $3p \leftrightarrow n, \varepsilon d$ are favored and the transitions $3p \leftrightarrow n, \varepsilon s$ are suppressed. Because the interaction between the $(^2D^o)nd\ ^3D^o$ states and the $(^4S^o)\varepsilon d\ ^3D^o$ continuum only contains favored transitions, the coupling matrix element is much bigger for these states than for the $(^2D^o)nd\ ^3S^o$ and $(^4S^o)\varepsilon s\ ^3S^o$ interaction or the $(^2D^o)ns\ ^3D^o$ and $(^4S^o)\varepsilon d\ ^3D^o$ interaction which both involve a propensity unfavored transition.

Another generic trend that can be explained by examining the $1/r_{ij}$ matrix element is the fact that the quan-

TABLE VI. A test run of different configuration lists. The quantum defect μ serves to show the convergence of a certain configuration. Only $^3S^o$ final state is shown. Core represents the configurations in Table I.

		Quantum defect μ				
Basis set	$3s^23p^3(^2D^o)nd\ ^3S^o$	$n=3$	4	5	6	7
HF[a]		0.014	0.027	0.032	0.034	0.036
HF+$(3s3p^33d+ns,nd)$		0.002	0.012	0.015	0.016	0.017
HF+$(3s^23p3d^2+ns,nd)$		0.004	0.012	0.015	0.017	0.018
HF+$(3s^23p^24f+ns,nd)$.		0.000	0.005	0.007	0.008	0.009
No. 1[b]		0.001	0.018	0.022	0.024	0.025
No. 2[c]		0.018	0.027	0.030	0.032	0.033
No. 3[d]		0.051	0.066	0.072	0.076	0.078
No. 4[e]		0.058	0.069	0.074	0.077	0.079
No. 5[f]		0.062	0.073	0.078	0.082	0.094
No. 6[g]		0.067	0.081	0.088	0.092	0.095
Exp.[h]		0.094	0.107	0.118	0.111	0.140

[a]HF = $3s^23p^3 + ns, nd$
[b]No. 1 = core + ns, nd.
[c]No. 2 = No. 1 + $(3s3p^4 + np, nf)$.
[d]No. 3 = No. 2 + $(3s^23p^23d + np, nf)$.
[e]No. 4 = No. 3 + $(3s^23p^24d + np, nf)$.
[f]No. 5 = No. 4 + $(3s3p^23d^2 + np)$.
[g]No. 6 = No. 5 + $(3s3p^23d^2+4f)$. This is also the configurations of the final state in our calculation.
[h]Experiment from Ref. [17]. We have switched the classification of $^3S^o$ and $^3D^o$. See explanation in text.

tum defect of the $(^2D^o)nd\ ^3S^o$ and $^3P^o$ states are smaller than the quantum defects of the $(^2P^o)nd\ ^3P^o$ and $^3D^o$ states which are smaller than the quantum defects for the $(^2D^o)nd\ ^3D^o$ states (see Fig. 3 and Tables IV and V). The quantum defects are related to the energy and are, therefore, related to the diagonal $1/r_{ij}$ matrix elements. The quantum defect increases when the energy (diagonal $1/r_{ij}$ matrix element) decreases. All of the terms of the $1/r_{ij}$ involving the outer d electron are the same except for the dipole and octupole exchange terms with the open p shell. We focus on these matrix elements since the only differences in binding energy can come from these terms. The radial matrix elements for all five of these channels are the same; the only difference between the channels is from the angular matrix elements. The exchange radial dipole matrix element is ~ 1.6 times larger than the radial octupole element; both matrix elements are positive. For both the $(^2D^o)nd\ ^3S^o$ and $^3P^o$ states, the angular dipole matrix element is roughly the same size as the angular octupole matrix element but of opposite sign which causes cancellation in the full $1/r_{ij}$ matrix element. For the other three channels, both of the angular matrix elements are negative with the $(^2D^o)nd\ ^3D^o$ matrix elements being ~ 2 times larger than those for the $(^2P^o)nd\ ^3P^o$ and $^3D^o$ states. This analysis indicates the $(^2D^o)nd\ ^3D^o$ states are more deeply bound than the $(^2P^o)nd\ ^3P^o$ and $^3D^o$ states which are more deeply bound than the $(^2D^o)nd\ ^3S^o$ and $^3P^o$ states. This ordering agrees with experiment and the full calculation.

VI. CONCLUSIONS

In the present work we have calculated the photoabsorption cross section of the chalcogen atoms from O to Te. The approximations that we have employed work well for the lighter atoms becoming progressively worse for the heavier atoms. By examining the matrix elements that couple the channels, we can explain some of the general trends of the spectra without resorting to huge calculations. Also, we have carried out a study of convergence of the wave function as different basis are added and have shown the importance of polarization-type basis functions to the description of the atomic dynamics.

ACKNOWLEDGMENTS

We thank M. Pindzola for providing us with a polarized $3d$ orbital for S in order to test convergence of our basis set. We also thank T. Gorczyca for helping us with the calculation of the ionic states. This work was partly supported by a grant from Auburn University and by a NSF Grant No. PHY9457903.

[1] R. B. Cairns and J. A. R. Samson, Phys. Rev. **139**, A1403 (1965).
[2] F. J. Comes, F. Speier, and A. Elzer, Z. Naturforsch. **23a**, 125 (1968).
[3] J. L. Kohl, G. P. Lafyatis, H. P. Palenius, and W. H. Parkinson, Phys. Rev. A **18**, 571 (1978).
[4] J. A. R. Samson and P. N. Pareek, Phys. Rev. A **31**, 1470 (1985).
[5] G. C. Angel and J. A. R. Samson, Phys. Rev. A **38**, 5578 (1988).
[6] R. E. Huffman, J. C. Larrabee, and Y. Tanaka, J. Chem. Phys. **46**, 2213 (1967).
[7] P. M. Dehmer, J. Berkowitz, and W. A. Chupka, J. Chem. Phys. **59**, 5777 (1973).
[8] K. T. Taylor and P. G. Burke, J. Phys. B **9**, L353 (1976).
[9] A. K. Pradhan and H. E. Saraph, J. Phys. B **10**, 3365 (1977).
[10] A. K. Pradhan, J. Phys. B **11**, L729 (1978).
[11] G. A. Vesnicheva, G. M. Malyshev, V. F. Orlov, and N. A. Cherepkov, Zh. Tekh. Fiz. **56**, 665 (1985) [Sov. Phys. Tech. Phys. **31**, 402 (1986)].
[12] R. P. Saxon, R. K. Nesbet, and C. J. Moble, Phys. Rev. A **39**, 1156 (1989).
[13] K. L. Bell, P. G. Burke, A. Hibbert, and A. E. Kingston, J. Phys. B **22**, 3197 (1989).
[14] M. J. Seaton, in *Recent Studies in Atomic and Molecular Processes*, edited by A. E. Kingston (Plenum, New York, 1987).
[15] S. S. Tayal, Phys. Rev. A **38**, 729 (1988).
[16] G. Tondello, Astrophys. J. **172**, 771 (1972).
[17] S. T. Gibson, J. P. Greene, B. Ruščić, and J. Berkowitz, J. Phys. B **19**, 2825 (1986).
[18] Y. N. Joshi, M. Mazzoni, A. Nencioni, W. H. Parkinson, and A. Cantu, J. Phys. B **20**, 1203 (1987).
[19] M. J. Conneely, K. Smith, and L. Lipsky, J. Phys. B **3**, 493 (1970).
[20] C. Mendoza and C. J. Zeippen, J. Phys. B **21**, 259 (1988).
[21] Z. Altun, J. Phys. B **25**, 2279 (1992).
[22] S. T. Gibson, J. P. Greene, B. Ruščić, and J. Berkowitz, J. Phys. B **19**, 2841 (1986).
[23] J. Berkowitz, C. H. Batson, and G. L. Goodman, Phys. Rev. A **24**, 149 (1981).
[24] F. Robicheaux and C. H. Greene, Phys. Rev. A **46**, 3821 (1992).
[25] F. Robicheaux and C. H. Greene, Phys. Rev. A **47**, 4908 (1993).
[26] C. Froese Fischer, Comput. Phys. Commun. **4**, 107 (1972).
[27] W. Johnson, D. Kohb, and K.-N. Huang, At. Data Nucl. Data Tables **28**, 333 (1983).
[28] B.I. Schneider, Chem. Phys. Lett. **31**, 237 (1975).
[29] F. Robicheaux, Phys. Rev. A **43**, 5946 (1991).
[30] U. Fano and A. R. P. Rau, *Atomic Collisions and Spectra* (Academic, Orlando, 1986); M. J. Seaton, Rep. Prog. Phys. **46**, 167 (1983).
[31] F. Robicheaux, Phys. Rev. A **48**, 4162 (1993).
[32] C. E. Moore, *Atomic Energy Levels*, Natl. Bur. Stand. Ref. Data Ser., Natl. Bur. Stand. (U.S.) Circ. No. 35 (U.S. GPO, Washington, DC, 1971), Vol. 1.
[33] D. Griffin and M. Pindzola (unpublished).
[34] M. Aymar, J. Phys. B **23**, 2697 (1990); C.H. Greene, Phys. Rev. A **42**, 1405 (1990).